Journal of Luminescence 161 (2015) 335–342

Contents lists available at ScienceDirect

Journal of Luminescence

journal homepage: www.elsevier.com/locate/jlumin

Preparation, characterization and photoluminescent studies of Cr and Nd co-doped Ce:YAG compounds

S.R. Naik [a], T. Shripathi [b], A.V. Salker [a,*]

[a] Department of Chemistry, Goa University, Goa 403206, India
[b] UGC-DAE Consortium for Scientific Research, Khandwa Road, Indore 452017, India

ARTICLE INFO

Article history:
Received 15 May 2013
Received in revised form
2 January 2015
Accepted 16 January 2015
Available online 28 January 2015

Keywords:
Sol–gel autocombustion
Yttrium Aluminum Garnet
Photoluminescence
Raman spectroscopy
XPS

ABSTRACT

Sol–gel autocombustion as an efficient method in the preparation of monophasic Cr and Nd co-doped Ce:YAG compounds has been demonstrated. A reduction in the formation temperature to 1000 °C as compared to the classical ceramic method has been effectively shown. Monophasic formation of the compounds has been confirmed from the X-ray diffraction study which is equally supported by the Raman spectroscopy. The TEM analysis confirms the formation of submicron sized particles (around 100 nm) which are equally supported by SEM micrographs revealing the granular morphology for the compounds. Photoluminescence (excitation) studies carried out for the compounds at 468, 341 and 685 nm display excellent emission intensity for the compounds with similar emission pattern pointing towards a common emission centre in all the three cases. Decrease in Ce^{3+} emission intensity for the Cr and Nd co-doped Ce:YAG is observed. Energy transfer mechanism is suggested for the lowering of emission intensity confirming the activity of Ce^{3+} as a sensitizer.

1. Introduction

White Light Emitting Diodes (WLED's) are replacing the classical lighting devices at a tremendous rate. These have various advantages over the other lighting sources in terms of the cost of manufacturing, output efficiency and are non-polluting sources of light energy. The demand for manufacturing of WLED's with better efficiency has led to the preparation of different oxide materials crystallizing into various crystal structures.

Doped Yttrium Aluminum Garnet, $Y_3Al_5O_{12}$ (YAG) is one of the most widely studied classes of phosphors. For example, Ce doped YAG exhibits excellent emission properties which enables its use in the manufacturing of yellow LED's showing emission in the range 480–670 nm [1–10]. It is also used in combination with blue light emitting diodes to produce WLED's [1,2,11–18]. YAG has been extensively studied by doping it with various metal ions at all the three sub lattices. Doped YAG is used in the manufacturing of LED's, display panels, lasers etc. whereas Nd doped YAG laser is used in the technological field [19–24]. Ho doped YAG is one of the prominent lasers for medical applications. Apart from these, Sm doped YAG also shows application for pressure calibration [25].

The luminescent properties exhibited by doped YAG compounds vary with the particle size of the compounds prepared. Large particles in the submicron range exhibit better luminescent properties as compared to the small ones (nanosized). This behavior in nano particles is due to the presence of a large number of defect sites which quench the luminescence [26]. But, submicron particles size prevents the application of these compounds as phosphors or other luminescent coatings, wherein the material is applied in the form of a thin film. Therefore it is necessary to prepare materials in the nano or submicron form to increase its applicability.

Sol–gel autocombustion is one of the widely used methods for the preparation of mixed metal oxides, viz: doped YIG, YAG, cobalt ferrites etc. [27–29]. Apart from sol–gel, other methods of preparation of doped YAG like ceramic, combustion, coprecipitation and precursor are also reported [2,11,13,16–18,22]. Among them sol–gel method is quite effective in obtaining a homogenous gel without any problem of cation segregation, thus yielding a monophasic end product. This paper reports a similar method for the compounds presented herein. Effectiveness of the malate–glycolate gel, the preparation conditions in yielding monophasic compounds and the photoluminescent properties of the compounds is very well explained herein. The paper provides an idea about the variation in emission intensity with changing dopant type (Nd or Cr) and energy transfer between ions in the excited state. This is aptly supported by the results obtained from the photoluminescence studies proving the role of Ce^{3+} ions as activators.

* Corresponding author. Tel.: +91 832 6519315; fax: +91 832 2452889.
E-mail address: sal_arun@rediffmail.com (A.V. Salker).

http://dx.doi.org/10.1016/j.jlumin.2015.01.040
0022-2313/

2. Experiment

2.1. Preparation

Sol–gel autocombustion method was utilized in the preparation of doped YAG. For the preparation of $Y_3Al_5O_{12}$, $Ce_{0.06}Y_{2.94}Al_5O_{12}$, $Ce_{0.06}Y_{2.88}Nd_{0.06}Al_5O_{12}$ and $Ce_{0.06}Y_{2.94}Al_{4.9975}Cr_{0.0025}O_{12}$, stoichiometric amounts of analytical grade $Ce(NO_3)_2 \cdot 6H_2O$ (Sigma-Aldrich), $Al(NO_3)_3 \cdot 9H_2O$ (Sigma-Aldrich), Y_2O_3 (Sigma-Aldrich), Nd_2O_3 (Molychem), and $Cr(NO_3)_3 \cdot H_2O$ (Sigma-Aldrich) were utilized. The water insoluble Y_2O_3 and Nd_2O_3 (For the Nd co-doped Ce:YAG) were brought into solution by dissolving in concentrated HNO_3 (A.R. Grade) with vigorous stirring on a hot plate maintained at temperature just around 100 °C. After obtaining a clear solution, $Ce(NO_3)_2 \cdot 6H_2O$, $Cr(NO_3)_3 \cdot H_2O$ (For the Cr co-doped Ce:YAG) and $Al(NO_3)_3 \cdot 9H_2O$ were added with continuous stirring. Calculated amount of malic acid (A.R. Grade) was then added (1:3 metal to malic acid ratio). The pH of the solution was adjusted to near neutral with 30% ammonia solution (A.R. Grade). A considerable change in color from colorless to yellow was observed which confirmed the chelating action of malic acid. The pH of solution was confirmed to be neutral after which ethylene glycol in the ratio 1:4 (with respect to malic acid) was added subsequently. The solution was then allowed to concentrate with continuous stirring. The gel so obtained was then transferred in a preheated oven (200 °C), wherein the contents were heated for 3 h. Formation of a voluminous foamy precursor was observed which was then crushed into fine powder with the help of an agate mortar and pestle. The precursor was then calcined at 400 °C for 4 h. It was homogenized with acetone and then sintered at 800 °C for 8 h. The obtained powder was then pelletized and further sintered at 1000 °C for 8 h. The as-prepared oxide samples were subjected to various characterization and solid state techniques.

2.2. Characterization

Crystalinity, crystal structure and phase purity of the powders were investigated by X-ray diffraction technique using Cu-Kα radiations of wavelength 1.5418 Å (filtered through Ni), in steps of 0.02 degrees on a RIGAKU ULTIMA IV X-ray diffractometer. Thermal behavior of the gel was studied in dry air utilizing a NETZCH STA 409 PC TG/DTA instrument at a rate of 10 °C min^{-1}. SHIMADZU FTIR PRESTIGE-21 spectrophotometer was put into use to record the vibrational modes of the compounds calcined at 1000 °C. The morphology analysis for the compounds was carried out on JEOL JSM-6360 LV Scanning electron microscope (SEM). Transmission Electron Microscopy (TEM) images were obtained using a TECNAI-G2-20 instrument operated at an accelerating voltage of 200 kV. Raman spectra were recorded in the backscattering geometry in the range 100–1000 cm^{-1} using a HORIBA JOBIN YVON HR-800 Raman spectrometer with an Olympus microscope (objective 50 ×) attachment and equipped with a CCD detector. A 488 nm Ar^+ and 633 nm He–Ne ion laser with 10 mW power was used as the excitation source for a spot about 1 mm in diameter. Background correction for all the spectra were carried out using Origin 8.0 software. For analysis, sample in the powder form was pressed in between two glass cover slips and analyzed. The valence states and the binding energies of various chemical species were determined by the X-ray Photoelectron Spectroscopy (XPS) employing VSW SCIENTIFIC INSTRUMENT with Al K_α as the incident source having incident energy of 1486.6 eV with a resolution of 0.9 eV. The absorbance measurements were carried out using a SHIMADZU UV-2450 UV–visible spectrometer equipped with a diffuse reflectance accessory in the wavelength range of 200–800 nm with $BaSO_4$ as a reference. Photoluminescence studies were carried out on SHIMADZU RF-5301PC spectroflurophotometer, with a Xenon flash lamp. The sample loaded on a powder holder provided by Shimadzu (the powder samples were densely packed on this holder) was mounted at about 45° to the excitation source for PL measurement. All samples were analyzed with the same slit width (1.5/1.5) to measure the excitation and emission spectra with wavelength resolution of 1 nm.

3. Results and discussion

3.1. TG–DTA analysis

The TG–DTA curves of $Y_{2.94}Ce_{0.06}Cr_{0.0025}Al_{4.9975}O_{12}$ (Cr co-doped Ce:YAG) malate–glycolate gel is shown in Fig. 1. The decomposition process can be divided into 4 major decomposition steps and can be described as follows. The dehydration process is observed at 120 °C with a mass loss of 13%. The major exotherm at 250 °C is the signature signal for the combustion reaction. A major mass loss of 47% is seen for this process which is due to the evolution of gaseous products like NH_3, NO_x and CO_2. The evolution of gases, trapped in the as-burnt matrix is observed around 400 °C which is seen as an exothermic signal in the figure, signifying the oxidation of residual carbon. A further oxidative decomposition of the carbonates is observed around 475 °C. This is an exothermic reaction associated with a mass loss of 8%. Beyond this a gradual mass loss takes place leaving behind an oxidized product with a residual mass of 2%.

3.2. X-ray analysis

X-ray diffractograms of the pristine and doped YAG compounds sintered at 1000 °C for 8 h are presented in Fig. 2(a). The peaks observed in the XRD patterns can be indexed to the characteristic planes of the cubic garnet structure. The phase analysis is carried out by matching the obtained diffractograms with the standard ICDD Card number 88-2047 characteristic of YAG and no extra peak signifying an impurity can be observed from the figure. The XRD peaks are broad in width signifying a fine nature of the particles. This can be confirmed from the TEM analysis. Peak broadening also signifies low density and a higher surface to volume ratio for the compounds. A shift in the peak position is observed with doping, suggesting a change in the lattice constant (a) with varying dopant type as shown in Fig. 2(b). Lattice constant (a) was determined for the (4 2 0) peak by equating miller indices and inter-planar distance (d). Formation of the monophasic compounds approves the sintering temperature to be appropriate.

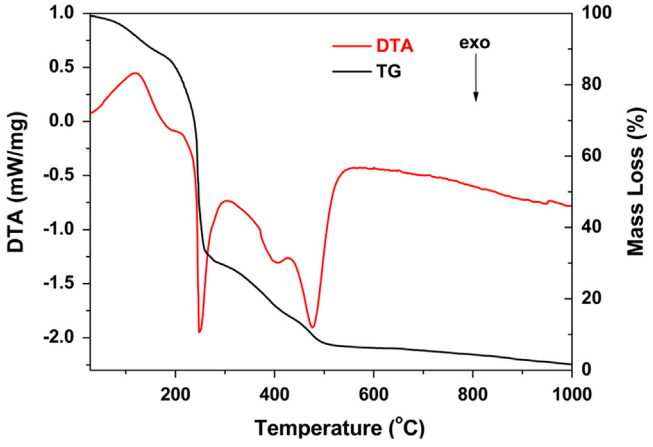

Fig. 1. TG–DTA curve of Cr co-doped Ce:YAG showing the thermal decomposition pattern of the gel in the temperature range of 28–1000 °C.

3.3. FTIR analysis

The FTIR spectra of doped YAG compounds in the range 350–1300 cm^{-1} are presented in Fig. 3. The spectra of the doped compounds match exactly with the pristine compound and no foreign peak for impurity can be observed from the profile of the compounds. Altogether three signals for Y–O stretching vibrations are observed at 478, 569 and 723 cm^{-1} [30]. Signals observed at 790 and 693 cm^{-1} are the stretching vibration of Al–O bond [31]. Apart from this, signals at 515 cm^{-1} are also observed for the pristine as well as the doped compounds, proving them to be the property of the garnet structure itself, and not as the sole representative stretching vibrations of Ce–O bond, as mentioned in the literature [32]. Since all these signals are shown by both the pristine and the doped compounds, these can be said to be the characteristic vibrational signals of the aluminum garnet structure as reported by other researchers [33]. The FTIR profile is found to remain unchanged with doping.

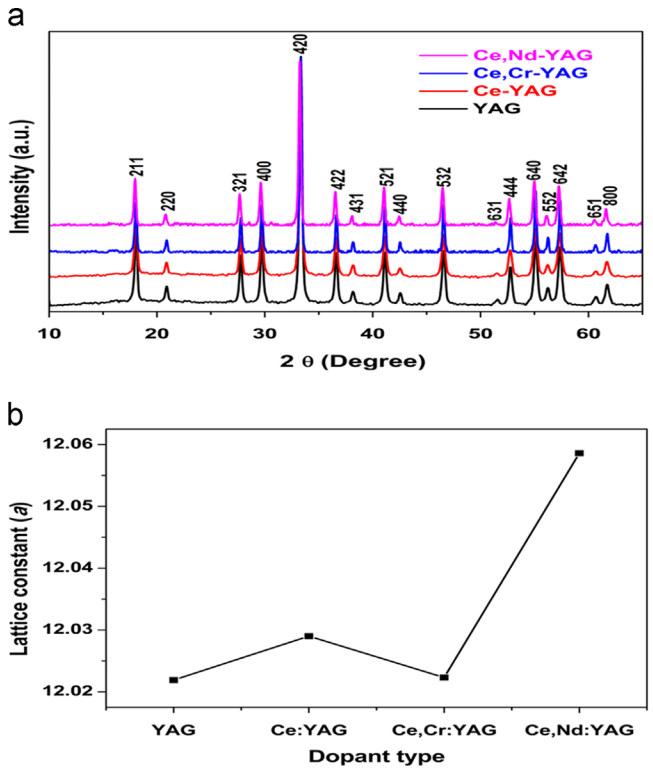

Fig. 2. X-ray Diffraction pattern of YAG, Ce:YAG, Nd co-doped Ce:YAG and Cr co-doped Ce:YAG powders are shown in (a), whereas the change in lattice constant with doping is shown in (b).

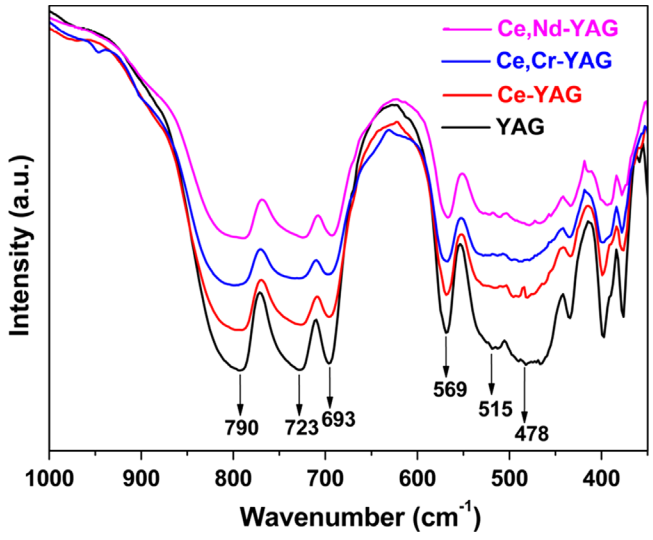

Fig. 3. FTIR spectra of YAG, Ce:YAG, Nd co-doped Ce:YAG and Cr co-doped Ce:YAG compounds sintered at 1000 °C for 8 h.

3.4. SEM analysis

SEM images of pristine and doped YAG compounds are shown in Fig. 4(a) and (b). The images reveal agglomerated masses of compounds which are further divided into finer particles revealing a non compact nature of the compounds. The images show similar morphology for both, pristine as well as doped YAG which do not suggest any change in morphology with doping.

3.5. TEM analysis

TEM images along with the electron diffraction (ED) patterns of YAG and Ce:YAG compounds are presented in Fig. 5(a)–(d). The images reveal the average particle size for the compounds to be around 100 nm with the presence of agglomerated particles. This is equally supported by the ED patterns showing well crystalline patterns and also supporting the agglomerated or fused nature of the particles. Overall, the TEM images reveal the particles of both the pristine and doped compounds to be similar in dimensions and no significant change in the morphology or particle size can be noticed with doping of Ce^{3+} ions.

3.6. Raman spectral analysis

Raman spectra of the pristine and Ce doped compounds are shown in Fig. 6(a) and (b). Pristine and doped YAG compounds belong to the cubic lattice with Ia3d space group symmetry. The unit cell consists of eight formula units of YAG. The Y^{3+} ions are situated in a closed cube surrounded by eight oxygen ions, resulting in a 24 distorted cubic symmetry (D_2), for the centrally located Y^{3+} ions at the dodecahedral site in the unit cell. Further, there are 24 (AlO_4) tetrahedra with S_4 symmetry of the central Al^{3+} ion and the other Al^{3+} ions occupy the 16 equivalent positions of C_{3i} symmetry at the octahedral site in the unit cell [34]. As mentioned in the literature, the vibrational spectra may be separated into internal modes of coordination (AlO_4) tetrahedron and lattice vibrational modes of the centrally located ions. There are in total 25 Raman-active modes for YAG with the (AlO_4) tetrahedron as the elementary unit [34]. Fig. 6(a) shows the spectrum of pristine YAG when analyzed with Ar^+ ion laser (488 nm) in the range 100–1700 cm^{-1}. The spectrum matches with that reported [34]. When analyzed with the Ar^+ ion laser, fluorescence is exhibited by the Ce^{3+} doped YAG which hampers the quality of spectrum. Therefore both the compounds are reanalysed using He–Ne ion laser (633 nm) in the range 700–2100 cm^{-1}. The spectra obtained for both pristine and Ce^{3+} doped, as shown in the Fig. 6(b) display similar pattern confirming no significant change in the structure of the compound with doping. But the Raman spectrum observed for pristine YAG compound using two different laser sources displayed non identical pattern which cannot be explained.

3.7. UV-DRS spectroscopy

The absorbance spectra of the pristine and doped YAG compounds are shown in the Fig. 7. The spectra reveal the absorbance pattern of the compounds in the range of wavelength from 200 to

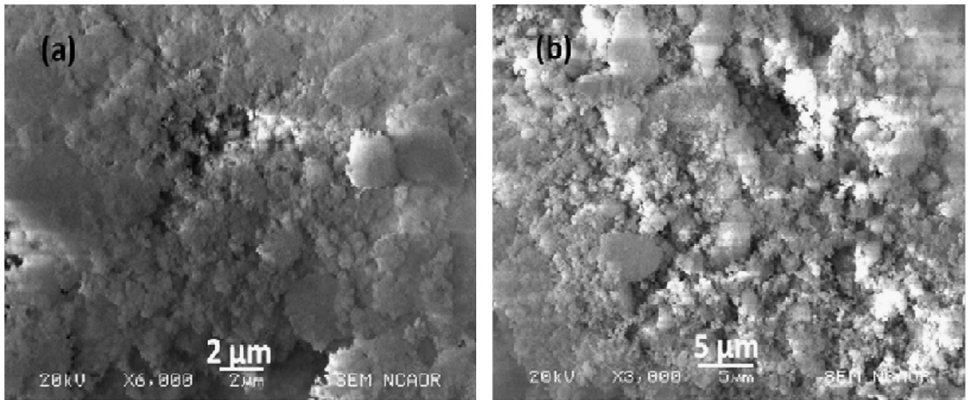

Fig. 4. SEM micrographs of (a) YAG, (b) Ce:YAG.

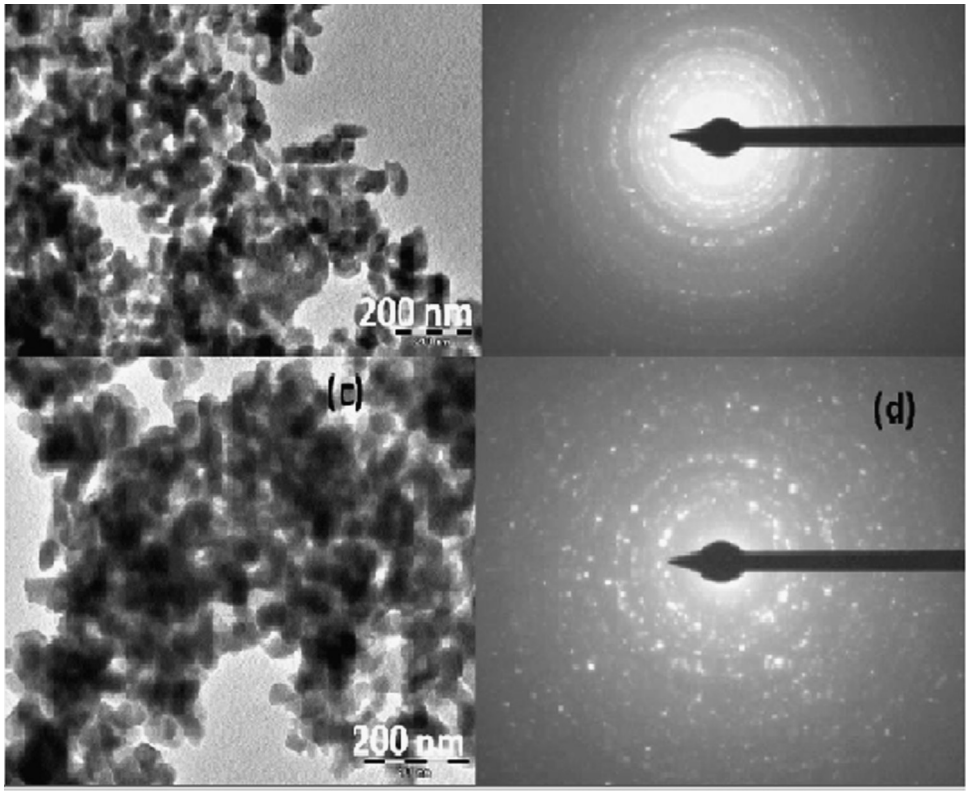

Fig. 5. TEM image and ED pattern of YAG is shown in (a) and (b), whereas TEM image of Ce:YAG along with ED is shown in (c) and (d).

800 nm. No absorption peaks are visible for the pristine compounds in the entire wavelength range, thus confirming the localized nature of the electrons in the compound. The dopants exhibit a quite different nature in the UV-visible region. A broad band ranging from 200 to 400 nm is seen for all the compounds. Variation in intensity of this band was observed with different dopants showing a maximum for Nd co-doped Ce:YAG compound and a minimum for Ce doped YAG. The absorbance spectra for the single and doubly doped compounds reveal the presence of a peak centered at 468 nm. Since the peak originates in the visible region and has a moderate intensity it can be termed as an f–d transition. This is the λ_{max} for the compounds and the same wavelength is used as the excitation wavelength for the photoluminescence studies.

3.8. Photoluminescence studies

The emission spectra of doped compounds with 468 nm as the excitation wavelength are displayed in Fig. 8(a). A broad emission band with its maxima at ~528 nm is observed from the figure. All the doped compounds show the maxima in the same region and blue shift in the maxima is observed with varying dopant type. A major difference in the intensity for the dopant type is observed. A maximum intensity is observed for Ce doped YAG, followed by Cr co-doped Ce:YAG, while Nd co-doped Ce:YAG showing the lowest intensity. Variation in intensity can be related to the enhancement or quenching of the emission centers with varying dopant type. Another factor responsible for the variation is the particle size of the compounds. As understood from the literature, a drop in luminescent intensity is expected with a decrease in the particle size. Smaller the particles, higher are the number of defects and therefore maximum quenching [26]. No major difference in the particle size of the compounds is seen from the TEM images thereby discarding any contribution of the particle size effect in varying luminescence intensity.

Fig. 8(a) shows the photoluminescence spectra of doped YAG compounds wherein a broad emission band nearly at 528 nm is

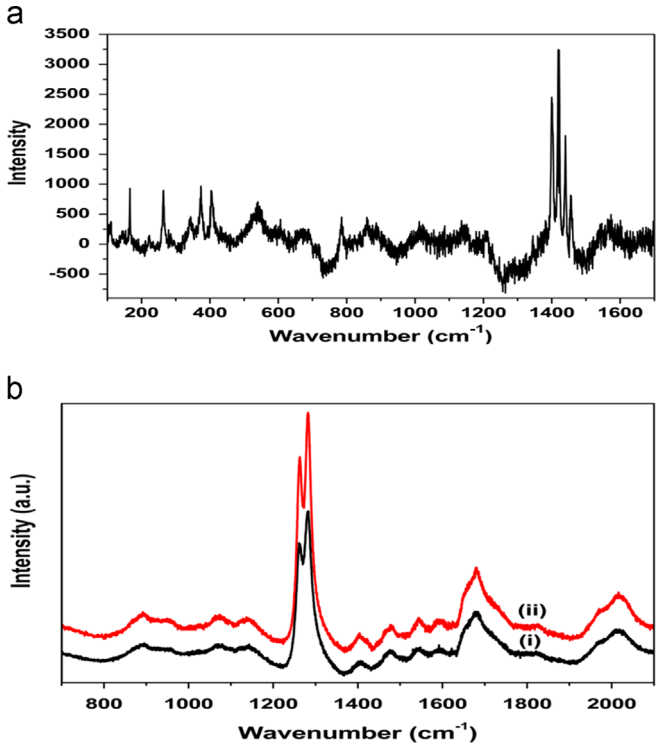

Fig. 6. Raman spectrum of pristine YAG when analyzed with Ar^+ ion laser (488 nm) in the range 100–1700 cm^{-1} is shown in (a), whereas (b) shows the Raman spectra of YAG and Ce:YAG with He–Ne ion laser (633 nm) in the range 700–2100 cm^{-1}.

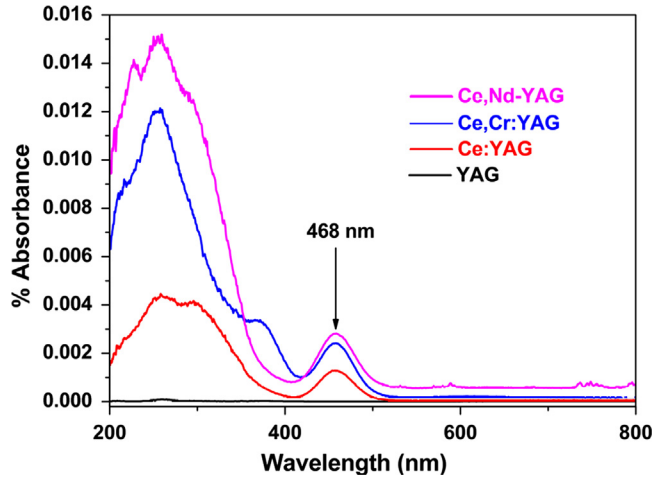

Fig. 7. Absorbance spectra of the pristine and doped YAG compounds in the range 200–800 nm.

observed. Bands at 341, 468 and 685 nm are observed in the excitation spectra upon keeping the emission wavelength of 528 nm as observed in Fig. 8(b). A free Ce^{3+} ion with $4f^1$ electronic configuration has two ground states, namely $^2F_{5/2}$ and $^2F_{7/2}$. Once the electron is excited from 4f to 5d sub-shell, the 5d electron of the exited $4f^05d^1$ configuration forms a ^2D term, which is split by spin–orbit coupling and two lower energy levels of $^2D_{3/2}$ and $^2D_{5/2}$ states are formed [12]. Therefore, the excitation bands peaked at 341 and 468 nm is attributed to $^2F_{5/2}$ (or $^2F_{7/2}$)→$^2D_{3/2}$ and $^2F_{5/2}$ (or $^2F_{7/2}$)→$^2D_{5/2}$ transition, respectively. Electrons on the higher energy level of $^2D_{5/2}$ state are unstable, which would relax to $^2D_{3/2}$ state with electron–phonon interaction. Therefore, the broad emission band in Fig. 8(a) is attributed to $^2D_{3/2}$→$^2F_{7/2}$ or $^2F_{5/2}$ transition. Since the radial wave function of the excited 5d electron extends spatially well beyond the closed $5s^25p^6$, its states are strongly perturbed by the crystal field. Thus, both the strongest excitation band and the strongest emission band are associated with the lowest-lying 5d state, which is affected by crystal field. A broad emission peak of Ce having highest intensity is observed in the experimental wavelength range for all the compounds. The deconvulated spectrum for the Ce doped YAG is presented in Fig. 8(c). The spectrum displays the two well separated emission peaks showing considerable difference in energy between them. Thus the high energy emission is attributed to the $^2D_{3/2}$→$^2F_{5/2}$ transition and the lower energy emission is attributed to the $^2D_{3/2}$→$^2F_{7/2}$ transition [12].

Fig. 8(a) shows the emission pattern of Cr co-doped Ce:YAG. The figure reveals the presence of a broad emission band for the Ce^{3+} state. Apart from this a small emission peak attributed to the Cr^{3+} state is seen at around 688 nm. Highly intense emission peak at around 690 is reported for the Ce and Cr co-doped YAG and singly doped Cr–YAG [11,34-36]. The doping concentration of Cr in the compound is 0.0025. Therefore peak of comparatively low intensity is seen for the compound reported herein. Cr has a ground state of $^4A_2$. With the laser light shining on it, the d electrons get promoted to $^4F_1$ and $^4F_2$ excited states. From here, the electrons undergo a rapid decay by a non-radiative process into a ^2E level. A radiative process occurs and gives rise to the 688 nm emission band via the ^2E→$^4A_2$ return to the ground state. The intensity of the peak representing the Ce emission decreases in intensity indicating energy transfer from Ce^{3+} to Cr^{3+} [11].

The emission spectrum of Nd co-doped Ce:YAG on 468 nm excitation is presented in Fig. 8(a). Decrease in the Ce^{3+} emission intensity band in comparison to the Ce doped YAG is observed which is similar to that of Cr co-doped Ce:YAG and is due to the energy transfer from Ce^{3+} to Nd^{3+} [37]. Nd^{3+} exhibits emission peaks past 900 nm which is beyond the range for the instrument utilized in this study.

The photoluminescent behavior of the compounds are also analyzed by exciting the compounds at 341 and 685 nm. The emission patterns of the compounds are shown in Fig. 8(d) and (e). Both the figures display similar patterns (lower intensity) matching with those observed when excited at 468 nm. An energy transfer from Ce^{3+} to the dopants can also be seen for these excitation wavelengths. A common emission centre is suggested to be the reason behind the display of similar emission patterns.

3.9. XPS spectroscopy

X-ray photoelectron spectroscopy is utilized as an effective tool in investigating the decrease in Ce^{3+} emission intensity observed for the Nd co-doped Ce:YAG. XPS spectra showing the full scan of the compound from 0 to 1400 eV is shown in Fig. 9(a). Fig. 9(b)–(f) shows the binding energies of (b) Y 3p, (c) Ce 3d, (d) Nd 3d, (e) Al 2p and (f) O 1s. Binding energy for the Y $3p_{1/2}$ and Y $3p_{3/2}$ states is seen at 311.89 and 300.02 eV, verifying the Y^{3+} state. Binding energy values of 902.06 and 885.46 eV for the Ce $3d_{3/2}$ and Ce $3d_{5/2}$ states is an indicative of the Ce^{3+} state. As seen from Fig. 9(d), binding energy values obtained for Nd $3d_{3/2}$ and Nd $3d_{5/2}$ are 998.52 and 981.26 eV respectively, confirming the trivalent state of neodymium ions in the compound. Apart from this, binding energy values obtained for the Al $2p_{3/2}$ and O1s states are 72.75 and 530.27 eV. An extra peak positioned at 531.07 eV is observed in the O 1s spectrum which can be attributed to the defect oxide or the surface oxygen ions with low coordination situation [29]. XPS analysis discards the formation of redox pairs of Ce^{4+}/Nd^{2+}, thus supporting the energy transfer process from the excited Ce^{3+} to the Nd^{3+} to be the reason behind the decrease observed in the Ce^{3+} emission intensity.

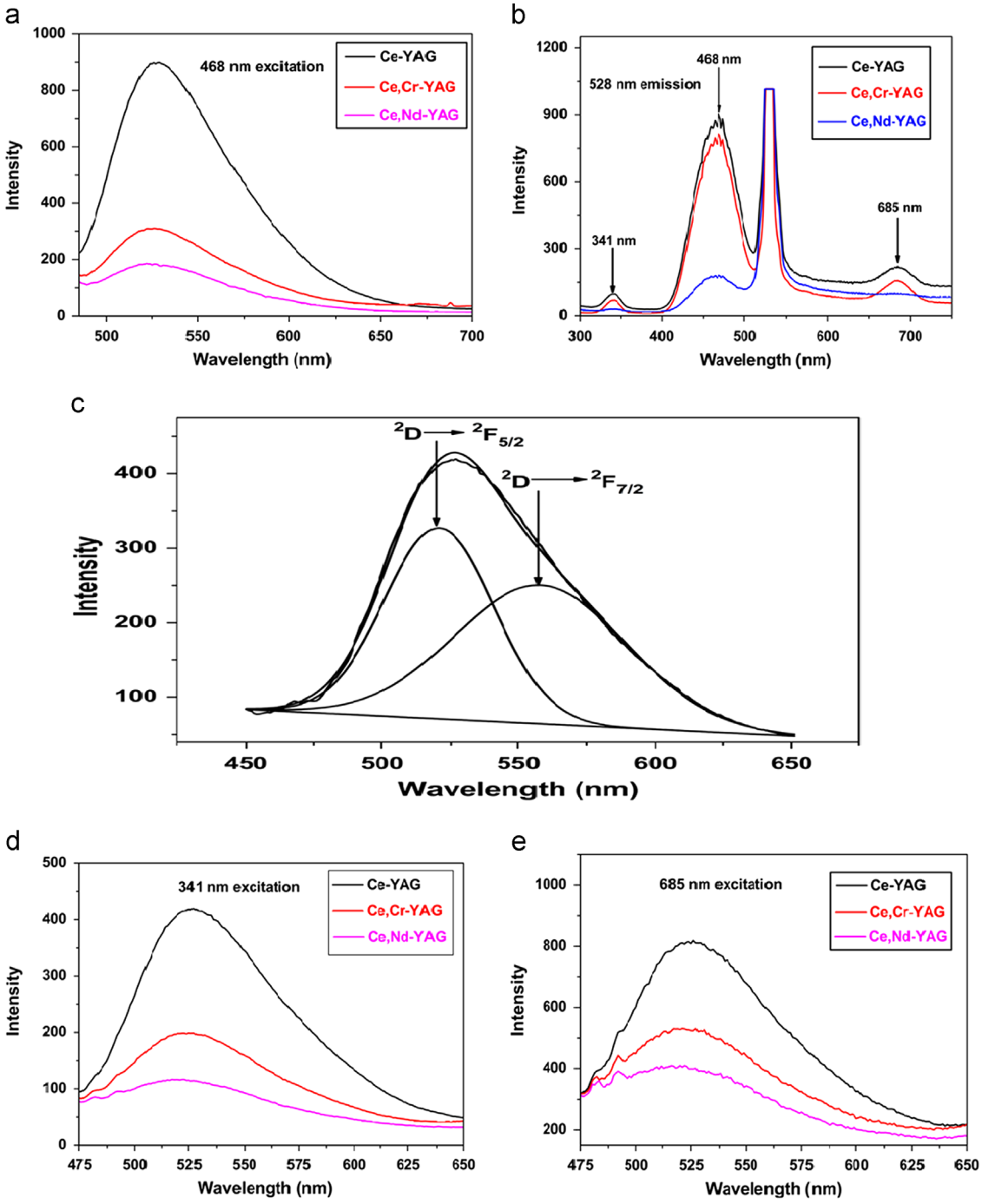

Fig. 8. Photoluminescence spectra of the compounds showing (a) 468 nm excitation, (b) 528 nm emission, (c) Deconvulated Ce^{3+} emission band, (d) 341 nm excitation and (e) 685 nm excitation.

4. Conclusion

Cr and Nd co-doped Ce:YAG compounds were successfully prepared by the sol–gel autocombustion method. The preparative conditions maintained throughout seemed to be appropriate in yielding monophasic compounds without any impurity phase, as confirmed from the XRD patterns. Formation of nanosized compounds averaging around 100 nm in size were confirmed from TEM images. Influence of doping on the Ce^{3+} emission was successfully studied for Cr and Nd co-doped Ce:YAG compounds. As understood from the results, decrease in intensity for the Ce^{3+} emission band was observed with doping, while Nd co-doped Ce:YAG showed the least emission intensity. A probable energy transfer from the excited Ce^{3+} ions to the Cr^{3+} and Nd^{3+} ions was suggested for the observed lowering in the intensity. It was successfully proved for the Cr co-doped Ce:YAG compound showing a small peak for the Cr^{3+} emission at 688 nm in the emission spectra. The probability of formation of redox pair (Ce^{4+}/Nd^{2+}) was discarded on the basis of XPS results showing the existence of trivalent state for both cerium and neodymium ions in the Nd co-doped Ce:YAG. Therefore, energy transfer from excited Ce^{3+} ions to the Nd^{3+} ions was suggested as an appropriate reason for the decrease observed in the emission intensity. Other than 468 nm excitation, other excitation wavelengths like 341 and 685 nm

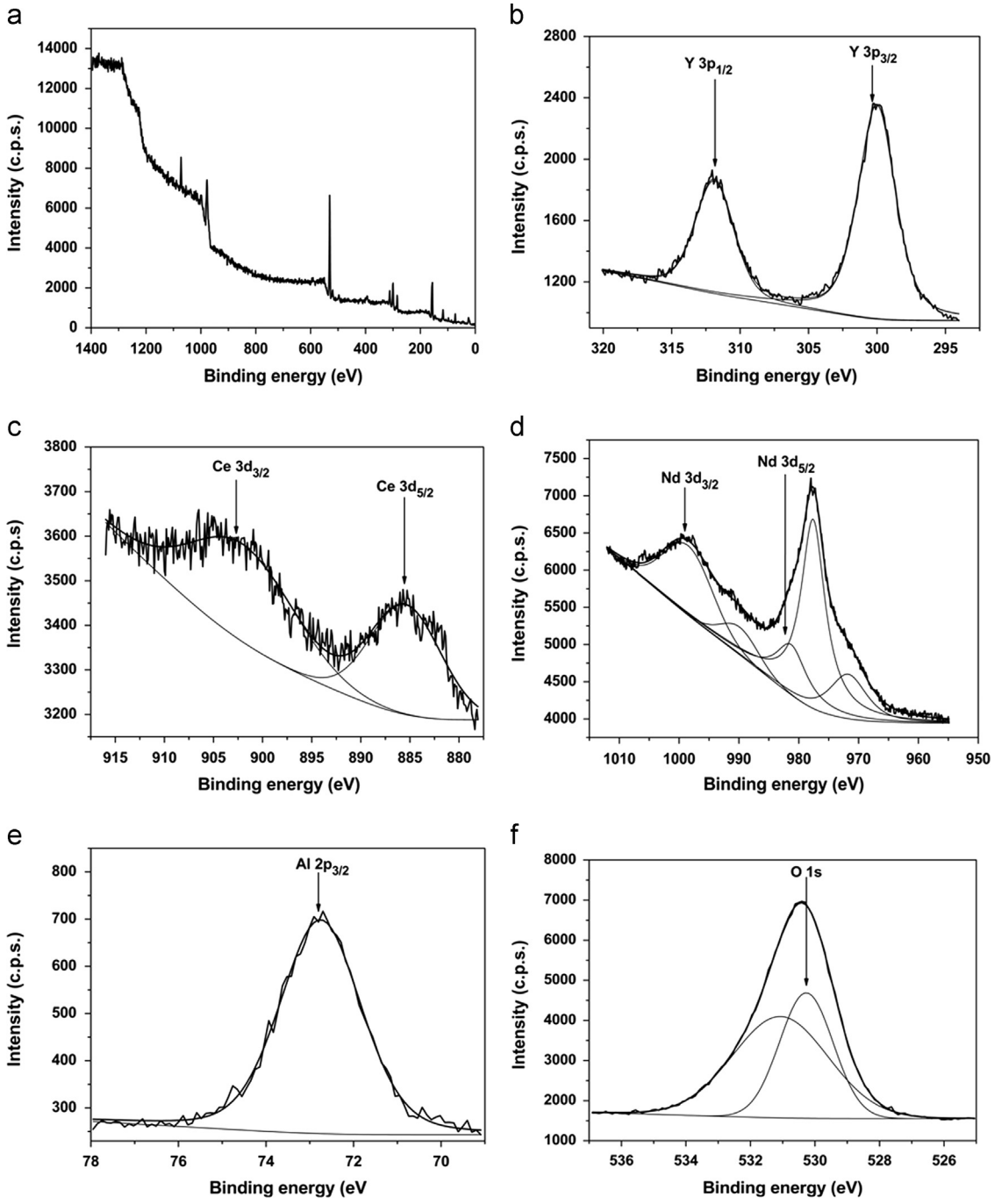

Fig. 9. XPS spectra of Nd co-doped Ce:YAG showing (a) FS, (b) Y 3p states, (c) Ce 3d states, (d) Nd 3d states, (e) Al 2p states and (f) O 1s state.

utilized, showed similar emission pattern, confirming the emission to take place from the same emission centre at all the three wavelengths.

Acknowledgment

S.R. Naik and A.V. Salker would like to acknowledge Dr. V.G. Sathe, Dr. N.P. Lalla and Dr. S. Tripathi (UGC-DAE Consortium for Scientific Research, Indore) for the Raman, TEM and XPS measurements. Authors are extremely grateful to Dr. Rahul Mohan and Ms. Sahina Gazi (NCAOR, Goa, India) for recording SEM images.

References

[1] M. Kottaisamy, P. Thiyagarajan, J. Mishra, M.S. Ramachandra Rao, Mater. Res. Bull. 43 (2008) 1657.
[2] Y. Pan, M. Wu, Q. Su, Mater. Sci. Eng. B 106 (2004) 251.
[3] H.M. Lee, C.C. Cheng, C.Y. Huang, Mater. Res. Bull. 44 (2009) 1081.
[4] S.M. Kaczmarek, G. Domianiak-Dzik, W. Ryba-Romanowski, J. Kisielewski, J. Wojtkowska, Cryst. Res. Technol. 34 (1999) 1031.
[5] C.H. Lua, R. Jagannathan, Appl. Phys. Lett. 80 (2002) 3608.
[6] X. Lia, H. Liu, J. Wang, H. Cui, F. Han, Mater. Res. Bull. 39 (2004) 1923.
[7] G. Del Rosario, S. Ohara, L. Mancic, O. Milosevic, Appl. Surf. Sci. 238 (2004) 469.
[8] R. Kasuya, T. Isobe, H. Kuma, J. Katano, J. Phys. Chem. B 109 (2005) 22126.
[9] A. Katelnikovas, P. Vitta, P. Pobedinskas, G. Tamulaitis, A. Žukauskasb J.E. Jorgensen, A. Kareiva, J. Cryst. Growth 304 (2007) 361.
[10] S. Mukherjee, V. Sudarsan, R.K. Vatsa, A.K. Tyagi, J. Lumin. 129 (2009) 69.

[11] W. Wang, J. Tang, S.T. (Victor) Hsu, J. Wang, B.P. Sullivan, Chem. Phys. Lett. 457 (2008) 103.
[12] L. Chen, C.C. Lin, C.W. Yeh, R.S. Liu, Materials 3 (2010) 2172.
[13] S.C. Huang, J.K. Wu, W.J. Hsu, H.H. Chang, H.Y. Hung, C.L. Lin, H.Y. Su, N. Bagkar, W.C. Ke, H.T. Kuo, R.S. Liu, Int. J. Appl. Ceram. Technol. 6 (2009) 465.
[14] Z. Na, W. Dajian, L. Lan, M. Yanshuang, Z. Xiaosong, M. Nan, J. Rare Earths 24 (2006) 294.
[15] C.H. Lu, H.C. Hong, R. Jagannathan, J. Mater. Chem. 12 (2002) 2525.
[16] E.N. Poddenezhnyi, A.O. Dobrodei, A.A. Boiko, A.V. Zdravkov, E.I. Grishkova, N. N. Khimich, Glass Phys. Chem. 37 (2011) 521.
[17] K. Zhang, W.B. Hu, Y.T. Wu, H.Z. Liu, Inorg. Mater. 44 (2008) 1218.
[18] K. Zhang, H. Liu, Y. Wu, W. Hu, J. Mater. Sci. 42 (2007) 9200.
[19] A. Ikesue, K. Yoshida, T. Yamamoto, I. Yamaga, J. Am. Ceram. Soc. 80 (1997) 1517.
[20] R. Huß, R. Wilhelm, C. Kolleck, J. Neumann, D. Kracht, Opt. Express 18 (2010) 13094.
[21] Y. Tang, X.Y. Zhang, Q.P. Wang, W.T. Wang, Z.G. Wu, L. Li, X.L. Zhang Y.G. Zhang, Z.J. Liu, X.H. Chen, S.Z. Fan, Laser Phys. 21 (2011) 695.
[22] Z. Xiaolin, L. Duo, W. Jiyang, Y. Haohai, Q. Haiming, S. Yuanhua, L. Hong, Rare Met. 30 (2011) 607.
[23] A. Benayas, E. Escuder, D. Jaque, Appl. Phys. B 107 (2012) 697.
[24] J. Li, Y. Wu, Y. Pan, W. Liu, L. An, S. Wang, J. Guo, Front. Chem. Eng. China 2 (2008) 248.
[25] C. Sanchez-Valle, I. Daniel, B. Reynard, R. Abraham, C. Goutaudier, J. Appl. Phys. 92 (2002) 4349.
[26] S. Zhou, Z. Fu, J. Zhang, S. Zhang, J. Lumin. 118 (2006) 179.
[27] S.R. Naik, A.V. Salker, J. Mater. Chem. 22 (2012) 2740.
[28] S.R. Naik, A.V. Salker, Phys. Chem. Chem. Phys. 14 (2012) 10032.
[29] S.R. Naik, A.V. Salker, S.M. Yusuf, S.S. Meena, J. Alloy. Compd. 566 (2013) 54.
[30] J. Li, J. Zhao, H. Zhou, J. Liang, X. Liu, B. Xu, Spectrochim. Acta A 78 (2011) 1310.
[31] A. Potdevin, G. Chadeyron, V. Briois, F. Leroux, C.V. Santilli, M. Dubois, D. Boyera, R. Mahiou, Dalton Trans. 39 (2010) 8706.
[32] N.N. Khimich, E.N. Poddenezhnyi, A.A. Boiko, A.V. Zdravkov, V.L. Ugolkov L.A. Koptelova, E.I. Grishkova, A.O. Dobrodei, Glass Phys. Chem. 35 (2009) 504.
[33] M. Chatterjee, M.K. Naskar, J. Am. Ceram. Soc. 89 (2006) 1443.
[34] Y.F. Chen, P.K. Lim, S.J. Lim, Y.J. Yang, L.J. Hu, H.P. Chiang, W.S. Tse, J. Raman Spectrosc. 34 (2003) 882.
[35] I. Matsubara, M. Paranthaman, S.W. Allison, M.R. Cates, D.L. Beshears D.E. Holcomb, Mater. Res. Bull. 35 (2000) 217.
[36] Y. Deng, Y.F. Guan, P.D. Rack, Thin Solid Films 515 (2006) 1721.
[37] P. Samuel, G.A. Kumar, T. Yanagitani, H. Yagi, K.I. Ueda, S.M. Babu, Opt. Mater. 34 (2011) 303.